

Control of Multi-Agent Formations with Only Shape Constraints †

H. Huang[‡], C. Yu* and Q. Wu[‡]

SUMMARY

This paper considers a novel problem of how to choose an appropriate geometry for a group of agents with only shape constraints but with a flexible scale. Instead of assigning the formation system with a specific geometry, here the only requirement on the desired geometry is a shape without any location, rotation and, most importantly, scale constraints. Optimal rigid transformation between two different geometries is discussed with especial focus on the scaling operation, and the cooperative performance of the system is evaluated by what we call the geometries *degrees of similarity* (DOS) with respect to the desired shape during the entire convergence process. The design of the scale when measuring the DOS is discussed from constant value and time-varying function perspectives respectively. Fixed structured nonlinear control laws that are functions on the scale are developed to guarantee the exponential convergence of the system to the assigned shape. Our research is originated from a three-agent formation system and is further extended to multiple ($n > 3$) agents by defining a *triangular complement graph*. Simulations demonstrate that formation system with the time-varying scale function outperforms the one with an arbitrary constant scale, and the relationship between underlying topology and the system performance is further discussed based on the simulation observations. Moreover, the control scheme is applied to bearing-only sensor-target localization to show its application potentials. Copyright © 2010 John Wiley & Sons, Ltd.

Received . . .

KEY WORDS: Multi-agent systems; Nonlinear formation control; Shape constraints.

1. INTRODUCTION

A group of agents working together in formation is seen in various field applications including, for example, spacecrafts exploring the deep space, underwater vehicles mapping out oceanbed and unmanned aerial vehicles detecting an unknown territory. Studies concerning this subject focus primarily on the stability of the formation systems where there are three well-known methodologies, namely distance-based formation control laws[1, 2], position-based control laws[3, 4, 5], and very recently, angle-based algorithms[6, 7]. Meanwhile, it is well known that the stability and the performance of the formation systems depend highly on the underlying communication topologies. This fact leads to the exploration of information flow laws among agents[8, 9] and the communication topology properties of the formation systems[10, 11]. Consequently there are control algorithms that aim to deal with various network dynamics[9, 12, 13].

Current research on formation control relies on the assumption that the desired geometry is specified, fixed, and known a priori either in a global coordinate or a local one. Inspired by the

*Correspondence to: Research School of Information Sciences and Engineering, The Australian National University, Canberra ACT 2600, Australia (Brad.yu@anu.edu.au)

†This work was completed during H. Huang's visit at The Australian National University which was supported by the University Fund of Beijing Institute of Technology. This work is also supported by the National Natural Science Foundation of China under grant 61074031. C. Yu is supported by the Australian Research Council through Queen Elizabeth II Fellowship under DP-110100538.

‡School of Automation, Beijing Institute of Technology, Beijing 100081, China (huanghuang.qinghew@bit.edu.cn)

fact that V-shaped formation provides birds with more aerodynamical and visual advantages than other types of flight in flocks[14], it is reasonable to conjecture that the geometry formed by the group of agents is closely related to the behaviors of the formation system. Thus with all those abundant results under the determined assumptions, we are now ready to move on to the next stage, that is, to consider situations where the only concern of the final state is the shape of the system rather than some specific geometry. In other words, this research considers the scenario where the requirement on the desired formation is its geometrical information without any constraints on its location, rotation and scale.

This particular problem arises in angle-based emitter-target localization that emerged in 1950s[15]. It were proved in [16], [17] and [18] that there were a set of geometries such as equilateral triangles in which sensors could provide the most accurate estimations of the target position. When the distances between sensors to the target are sufficiently larger than the ones between sensors, the shape formed by the group of agents is then the major concern instead of a specific geometry. It can be further verified that the geometry with a higher degree of similarity (DOS) (please refer to Section 3 for its definition) to the optimal shape can provide better target location estimation. Thus *in order to improve the accuracy of measurements on the target before sensors reaching the desired shape so as to allow more time for strategy making, a formation system that maintains a high DOS to the optimal shape during convergence is more preferable than simply focusing on the final shape.*

However, despite of the potential advantages brought by the geometrical resemblance, optimal formation control with only shape constraints has not yet received enough attentions. To our best knowledge, there are only a few literatures that are *related* to this topic. One was reported in [19] where the authors focused on finding the optimal scale of the prescribed shape for a set of robots such that the total distance they traveled was minimized. However, robot control during the process was ignored and thus the group of robots did not exhibit any cooperative behaviors. In another work[20] on optimal relative formation control of three wheeled robots, the cost function was the kinematic energy sum of the three robots. By choosing a robot as the rotation center, the optimal relative positions of robots were designed. Shape control irrespective of any objectives is seen in a small number of literatures. By modeling each agent as a double integrator, reference [21] considered shape control on the projected orthogonal reference frame, and very recently, reference [7] proposed a distributed algorithm that stabilized three agents in the assigned shape. However, those research ignored the performance during the convergence process and thus are not favorable to tasks such as sensor-target localization.

To this end, this paper aims to explore the novel topic of formation control under only shape constraints, and exploit the design of scales that provide the optimal rigid transformation(rotation, translation and scaling operations) between two different geometries. The objective is to minimize a cost function that integrates the difference between the geometry and the desired shape over the entire convergence process. Although there are quite a few discussions on the optimal formation control, the objectives are normally fuel consumption[22], traveling length and time[23]. Fixed structured nonlinear control laws on the edge state and the pending scale are proposed. When choosing the appropriate scale of the final geometry so as to minimize the cost value, two situations are considered one of which is to determine an optimal value a priori and set it constant during the entire process. Another more intelligent method is to design a function named the scale function that adjusts the scale online.

Here is an outline of the paper: Section II contains the notations and definitions that are used in the paper. A nonlinear control law, which is the starting point of this research, is introduced in this section as well. In Section III, the difference between two geometries is defined and further the cost function is proposed which represents the geometrical performance during formation attainment. Design of a constant scale is discussed in Section IV, and in Section V a scale function is proposed that further reduces the minimum from the previous section. By defining a *triangular complement graph* of the minimally rigid graph, the algorithm applies to multiple ($n > 3$) agents case as well. In order to broaden the application of the nonlinear algorithm to situations with determined final geometries, controllability of the system is discussed by adding a positive weight factor to the nonlinear control law. Moreover, applications of the proposed control schema in sensor-target

localization are presented in Section VI. Section VII presents extensive experimental simulations that verify the effectiveness of the algorithm and show its application potentials. Conclusions are made in Section VIII.

2. PRELIMINARY

Positive real numbers are denoted by \mathbb{R}^+ and a matrix of size $m \times n$ is denoted by $\mathbb{R}^{m \times n}$ where when $n = 1$, it is always abbreviated by \mathbb{R}^m . The (block) diagonal matrix of vector \mathbf{v} is denoted by $\text{diag}(v_i)$ with (vector) v_i being the i th (block) diagonal entry. Sometimes we may also use $\text{diag}(v_1, \dots, v_n)$ instead.

For an undirected graph $G = (V, E)$, the numbers of edges and vertices are denoted by $|E|$ and $|V|$ respectively. Vertex i is the neighbor of vertex j , denoted by $i \sim j$, if they are connected by an edge in E . Edge i is the neighbor of edge j if they share a vertex. The neighbor sets of vertex i and edge i are denoted by $\mathcal{N}_v(i)$ and $\mathcal{N}_e(i)$ respectively. The minimal distance between vertex i and vertex j is the minimal number of edges in E that are needed to have them connected.

Throughout the paper, we focus on 2D formations on a plane, and we do not consider a system where agents are collinear or coincided, that is

Assumption 2.1

The initial positions and the desired positions of agents in a formation system are non-collinear.

For graph G , if we label the nodes in V from 1 to $|V|$ and the edges in E from 1 to $|E|$, the *representation* of G is a vector \mathbf{z} whose i th entry $z_i \in \mathbb{R}^2$ is the position of the i th node. Given G , if we assign an arbitrary direction on each edge, then the representation \mathbf{z} uniquely determines an edge vector \mathbf{e} where $e_i \in \mathbb{R}^2$ corresponds to the i th directed edge in E , and \mathbf{e} is called a *relative representation* or a *geometry* of G . Note that in this paper, a geometry is associated with a graph, which is a more strict definition than that of a polygon. Given a graph G , the distance between two representations \mathbf{z}_1 and \mathbf{z}_2 is $d(\mathbf{z}_1, \mathbf{z}_2) = \max_{i \in V} \|z_{1i} - z_{2i}\|$. The representation \mathbf{z} is further called a *realization* of G if all the distances between neighboring vertexes in G are compatible, and consequentially \mathbf{e} is the *relative realization* of G . All possible realizations of G form a vector space denoted by \mathbb{Z} , and consequently a link/edge space \mathbb{E} . A *formation* system is a group of agents that communicate over G and whose deployment is depicted by a realization of G .

A realization \mathbf{z} of G in two dimensions is rigid if there exists $\varepsilon > 0$ such that for all realizations $\mathbf{z}' \in \mathbb{Z}$ that satisfy $\|z'_i - z'_j\| = \|z_i - z_j\|, \forall i \sim j$ and $d(\mathbf{z}, \mathbf{z}') < \varepsilon$, there holds $\|z'_i - z'_j\| = \|z_i - z_j\|, \forall i, j \in V$. A rigid graph is further minimally rigid if no single edge can be removed without losing rigidity. Finally, a globally rigid graph G is a graph where $\|z'_i - z'_j\| = \|z_i - z_j\|, \forall i, j \in V$ holds for an arbitrary $\varepsilon > 0$. More rigorous definitions could be found, for example, in [3, 10].

Given a graph G and two realizations \mathbf{z}_d and \mathbf{z} , \mathbf{z} is *similar* to \mathbf{z}_d if

$$\frac{\|z_l - z_m\|}{\|z_1 - z_2\|} = \frac{\|z_{d_l} - z_{d_m}\|}{\|z_{d_1} - z_{d_2}\|}, \forall l, m \in V \quad (1)$$

and consequently, \mathbf{e} and \mathbf{e}_d are *similar* geometries. Without lose of generality, assume node 1 in both realizations is deployed at the origin. Then it is necessary that

$$\mathbf{z}_{d_i} = kO(\theta)\mathbf{z}_i \quad (2)$$

where $k \in \mathbb{R}$ and $O(\theta)$ is a rotation transformation through angle θ . Fig. 1(a) and Fig. 1(b) give examples showing similar and dissimilar geometries. Although the two triangles in Fig. 1(b) are similar ones in the usual sense of plane geometry, in our case this is no longer true due to the mismatching of indexed nodes.

Given a relative realization \mathbf{e}_d of G , a shape vector $S(\mathbf{e}_d)$ generated from \mathbf{e}_d is determined by

$$S(\mathbf{e}_d) = [s_1 \quad s_2 \quad \dots \quad s_l]^T \in \mathbb{R}^l, l = |E|, s_i \in \mathbb{R}^+$$

where $s_i = \|e_{d_i}\|$. In most of cases, we will use S for abbreviation. The set $\{\mathbf{e}|S\}$ consists of all similar geometries to S over the same graph. Fig. 2 gives an explanation on the relationships between

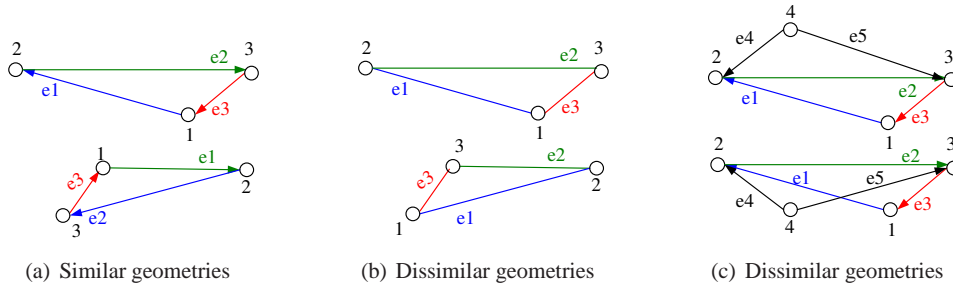


Figure 1. Geometries with ordered vertexes

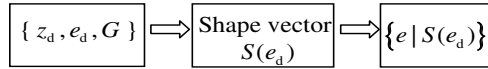


Figure 2. The relationship between the shape and the geometry

those three notations. Elements are uniquely determined along the arrows and the reverse is not true. In fact, given a shape vector S , it uniquely determines a shape or a geometry e_d if and only if the underlying graph is a globally rigid one[10].

Due to the nature of the algorithms introduced in this paper and for convenience, the scale of a geometry in $\{e|S\}$ with respect to S is

$$s = \frac{\|e_1\|^2}{2s_1^2}$$

which is identical to all edges.

The incidence matrix is frequently used to describe the structure of a directed graph. For an undirected graph, by assigning each edge an arbitrary direction, we have the oriented incidence matrix as seen, for example, in [24].

Definition 2.1 (Oriented Incidence Matrix)

For an undirected graph $G = (V, E)$, each edge is assigned with a random direction to generate a directed graph $\bar{G} = (V, \bar{E})$. The oriented incidence matrix of G , denoted by $H(G)$, is a matrix of dimension $|E| \times |V|$ whose i th row corresponds to the i th edge in \bar{E} with entries

$$h_{ij} = \begin{cases} 1 & , \bar{e}_i \text{ sinks at } j \\ -1 & , \bar{e}_i \text{ leaves } j \\ 0 & , \text{others} \end{cases}$$

Lemma 2.1

The oriented incidence matrix $H(G)$ has rank $n - 1$ when G is connected.

By introducing the expended incidence matrix $\hat{H} = H \otimes I_2$, where \otimes is the Kronecker product, the edge space \mathbb{E} can then be considered as a codomain of \hat{H} from the vector space \mathbb{Z} :

$$\mathbf{e} = \hat{H}\mathbf{z}$$

where $\mathbf{z} \in \mathbb{Z}$ and $\mathbf{e} \in \mathbb{E}$. Thus we have $\mathbf{e} \in \text{Im}\hat{H}$.

Further we define a rigidity function[3] (also known as the edge function[25])

$$\bar{\mathbf{z}} = r(\mathbf{e}) = \frac{1}{2} [\|e_1\|^2 \quad \cdots \quad \|e_m\|^2]^T \quad (3)$$

and the rigidity matrix is further defined as

$$R(\mathbf{e}) = \frac{\partial \bar{\mathbf{z}}}{\partial \mathbf{z}} = \Lambda(\mathbf{e})^T \hat{H}$$

with $\Lambda(\mathbf{e}) = \text{diag}(e_k)$, $e_k \in \mathbb{R}^2$. For a rigid graph, $\text{rank}R(\mathbf{e}) = 2|E| - 3$.

Lemma 2.2 ([25])

For a desired relative realization \mathbf{e}_d over $G = (V, E)$ and the vector $\mathbf{d} \in \mathbb{R}^{|E|}$ with $d_k = [\frac{1}{2}\|e_{d_k}\|^2]$, by choosing the potential function

$$V(\mathbf{e}) = \sum_{k=1}^{|E|} \frac{1}{8} (\|e_k\|^2 - 2d_k)^2 \quad (4)$$

the control law

$$\dot{\mathbf{z}} = u = -\hat{H}^T [\partial V(\mathbf{e}) / \partial \mathbf{e}]^T \quad (5)$$

is an *inverse* optimal solution to the optimization problem

$$\begin{aligned} \min \bar{J}(\mathbf{e}_0, u) &= \frac{1}{2} \int_0^\infty \|R(\mathbf{e})^T [r(\mathbf{e}) - \mathbf{d}]\|^2 + \|u\|^2 d\tau \\ \text{s.t. } \dot{\mathbf{e}} &= \hat{H}u, \mathbf{e}_0 = \mathbf{e}(0) \in \text{Im}\hat{H} \end{aligned} \quad (6)$$

and the formation system converges to the largest invariant set

$$\mathcal{I}_e = \{\mathbf{e} \in \text{Im}\hat{H} : V(\mathbf{e}) < V(\mathbf{e}_0), \|R(\mathbf{e})^T [r(\mathbf{e}) - \mathbf{d}]\| = 0\} \quad (7)$$

The proof of the lemma is based on the Hamilton-Jacobi-Bellman (HJB) equation and Lyapunov Theory. For details please refer to [25].

Algorithm (5) requires that each agent has the knowledge of the global coordinates of its neighbors. This requirement is also assumed to be true in our research.

3. COST FUNCTION AND COOPERATIVE PERFORMANCE

With the wide range of applications of sensor networks, the geometric characters of a group of sensors are sometimes crucial to the achievement of tasks, such as bearing only sensor-target localization, shape-constrained formation reconfiguration and obstacle avoidance. Thus it is exigent to propose an efficient way to distinguish two geometries.

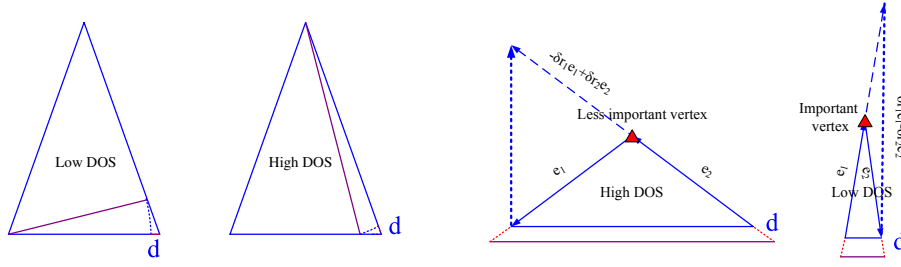
In image processing, especially in pattern matching, the Hausdorff distance is commonly used to evaluate how much do two geometries resemble each other under rigid transformation[26]. The problem of shape matching is to find the optimal transformation that minimizes the distance. Sometimes points on the edges are assigned with different weights indicating their importance to the shape. However, the Hausdorff distance metric is on the basis a minimization function, which is not favorable as an objective function. Meanwhile, at each time step, the time complexity to compute the Hausdorff distance for two points sets of size p and q is $O(pq)$. Thus another metric function is expected that produces intuitively reasonable results and is beneficial to optimization.

Before we dive into the mathematical formalizations, here are two observations for determining the resemblance of geometries with respect to the reference/desired shape:

- i A geometry is less sensitive to perturbations on *long* edges
- ii A geometry is less sensitive to perturbations on edges with large included angles $(0, \pi)$

Fig. 3 further explains the above two observations. It is intuitive that under the same perturbation, the long edge bring small deformation to the geometry than that of a short edge, as the two geometries in Fig. 3(a). Meanwhile, apart from the lengths of edges, another profile of a shape is the vertex, especially those sharp vertexes, i.e., the included angle of the two edges adjacent at the vertex is small.

When two geometries are similar to each other, the scale between them is the ratio of two corresponding edges in the geometries and is identical to all the pairs of edges. However, for two dissimilar geometries, there is no common ratio for any pairs of edges, thus choosing an appropriate scale is premise to the analysis of geometries resemblance.



(a) When the short edge suffer a small perturbation, the (b) When the angle included in the two edges is perturbed geometry varies a lot w.r.t. the nominal one; large(0π), perturbations on the two edges will result in When the same perturbation is added to the long edge, small change to shape; When the angle is small(0π), the new geometry is quite close to the nominal one the shape is greatly affected by the same perturbations

Figure 3. The sensitivity of a geometry

According to the above two observations, it is obviously inappropriate to simply use the differences between edges lengths of the two geometries to measure how two geometries are related:

$$J' = \int_0^\infty \|r(\mathbf{e}) - r(\mathbf{e}')\|^2 d\tau \quad (8)$$

because J' does not consider observation i or observation ii .

We are interested in the resemblance of two geometries, thus under observations i and ii , the difference between geometry \mathbf{e} and \mathbf{e}' is

$$\rho_\Theta(\mathbf{e}, \mathbf{e}') = H^T \begin{bmatrix} (r_1(\mathbf{e}) - \Theta r_1(\mathbf{e}'))e_1 \\ \vdots \\ (r_n(\mathbf{e}) - \Theta r_n(\mathbf{e}'))e_n \end{bmatrix}$$

As one can tell, an appropriate scale Θ is key to the evaluation. In our research, the geometry is depicted by $2|V| - 3$ directed edges rather than the coordinates of the vertices, thus the translation and rotation operations are not our concerns. The element $(r_i(\mathbf{e}) - \Theta r_i(\mathbf{e}'))e_i := \delta r_i e_i$ indicates that each edge in one geometry is scaled by the edge difference between the two geometries. This is designed to take care of observation i . Inspired by the weighted Hausdorff distance, we introduce the transformation H^T which allows two neighboring edges communicate and consequently, as shown in Fig. 3(b), evolve into the edges in dot lines, the lengths of which are positive monotony to the sharpness of the vertices.

Given a geometry \mathbf{e} and a shape $S(\mathbf{e}')$, the degree of similarity (DOS) of \mathbf{e} with respect to S is measured by

$$dos_\Theta(\mathbf{e}, S(\mathbf{e}')) = \|\rho_\Theta(\mathbf{e}, \mathbf{e}')\|_2^{-2} \quad (9)$$

A geometry with a higher DOS to S is said to be more resemble to S . When the geometry is similar to S , $dos_\Theta(\mathbf{e}, \mathbf{e}') \rightarrow \infty$.

As mentioned before, by taking care of the geometries DOS during the entire convergence, sensors can provide reliable measurement of the target in an early stage. Thus in this research, the *geometrical performance of a formation system is the integral of the DOS with respect to the desired shape during convergence*:

$$J(\mathbf{e}_0, u, \Theta) = \int_0^\infty dos_\Theta^{-1}(\mathbf{e}, S(\mathbf{e}')) d\tau = \int_0^\infty \|R(\mathbf{e})^T [r(\mathbf{e}) - \Theta \bar{S}]\|^2 d\tau \quad (10)$$

with $\bar{S} = [\bar{s}_i]$ and $\bar{s}_i = s_i^2$. We use S^2 instead of S due to the composition of $r(\mathbf{e})$ in (3). Apart from the initial state \mathbf{e}_0 and the control law u , the value of J is also a function on the scale Θ .

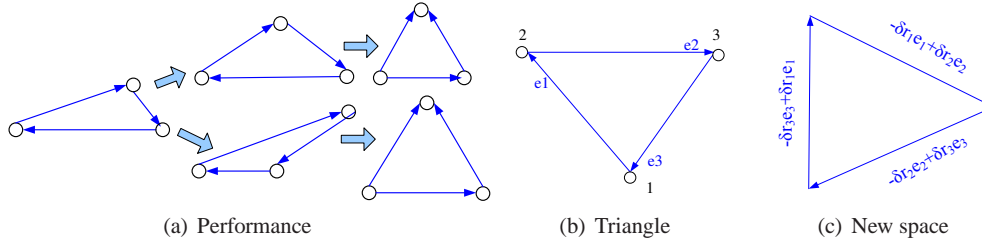


Figure 4. Triangular geometry of three agents. For the definitions of DOS, please refer to (9)

For example we consider three agents in a formation as shown in Fig. 4(b). If we set $\delta r_i = r_i - \Theta \bar{s}_i$ and denote $L = \|R(\mathbf{e})^T[r(\mathbf{e}) - \Theta \bar{S}]\|^2$, it yields

$$\begin{aligned} L &= \|\hat{H}^T [\delta r_1 e_1 \quad \cdots \quad \delta r_n e_n]^T\|^2 \\ &= \|\delta r_1 e_1 - \delta r_2 e_2\|^2 + \|\delta r_2 e_2 - \delta r_3 e_3\|^2 + \|\delta r_3 e_3 - \delta r_1 e_1\|^2 \end{aligned} \quad (11)$$

The value of L is the sum of lengths of the three new vectors in Fig. 4(c).

Remark 3.1

A formation system with a smaller cost value (10) is considered to exhibit better geometrical/cooperative performance during convergence.

By minimizing the cost function (10), the two situations as, for example, the ones in Fig. 4(a), are expected to be distinguished. The upper case has better geometric performance as the geometries during convergence have consistently high DOS with respect to the desired shape. For the bottom situation, although the three agents attain the desired geometry, it differs a lot from the desired shape during the process. In sensor networks for localization, formation system in the upper case may allow sensors to provide some rough estimate of the target before attaining the formation. We will show this later through experimental results in Section 7.

When the underlying graph of the formation system is a minimally rigid graph, the convergence of J is equivalent to $r(\mathbf{e}) \rightarrow \Theta \bar{S}$. Two forms of Θ are considered in this paper, namely Θ being constant: $\Theta = s_c \in \mathbb{R}^+$, and Θ being a time-varying function on \mathbf{e} : $\Theta = \tilde{s}(\mathbf{e}) \in C(\mathbb{E})$, where C is the set of continuous mappings. The cost functions are then written, respectively, as:

$$J_c(\mathbf{e}_0, u, s_c) = \int_0^\infty \|R(\mathbf{e})^T[r(\mathbf{e}) - s_c \bar{S}]\|^2 d\tau \quad (12)$$

and

$$J_v(\mathbf{e}_0, u, \tilde{s}(\mathbf{e})) = \int_0^\infty \|R(\mathbf{e})^T[r(\mathbf{e}) - \tilde{s}(\mathbf{e}) \bar{S}]\|^2 d\tau \quad (13)$$

The main concern in this research is the determination of s_c and $\tilde{s}(\mathbf{e})$ such that the cost functions J_c and J_v are minimized. Note that J_c and J_v are not just quadratic expressions but a function on \mathbf{e}_0 , u and s_c or $\tilde{s}(\mathbf{e})$, thus minimizing the values of J_c and J_v is not trivial. Inspired by the control law in Lemma 2.2, in this research, we will fix the structure of the control law and focus on the design of the optimal scale function.

Problem 3.1

Consider a formation system where each agent is modeled by

$$\dot{\mathbf{z}} = u \quad (14)$$

and the underlying graph G is a minimally rigid graph.

- Let $\Theta = s_c \in \mathbb{R}^+$, and consider the following control law on s_c and \mathbf{e} :

$$u(s_c, \mathbf{e}) = -R^T(\mathbf{e})[r(\mathbf{e}) - s_c \bar{S}]. \quad (15)$$

Find the optimal value of s_c such that $\mathbf{e}_f \in \{\mathbf{e}|S\}$ where \mathbf{e}_f is the stable realization and

$$J_c^*(\mathbf{e}_0, u(s_c, \mathbf{e})) = \min_{s_c \in \mathbb{R}^+} J_c(\mathbf{e}_0, u(s_c, \mathbf{e}), s_c) \quad (16)$$

- Let $\Theta = \tilde{s}(\mathbf{e})$ where $\tilde{s} \in C(\mathbb{E})$, and consider the following control law on $\tilde{s}(\mathbf{e})$ and \mathbf{e} :

$$u(\tilde{s}(\mathbf{e}), \mathbf{e}) = -R(\mathbf{e})^T M(\mathbf{e})^T [r(\mathbf{e}) - \tilde{s}(\mathbf{e})\bar{S}]. \quad (17)$$

Find the control gain $M(\mathbf{e}) \in \mathbb{R}^{(2n-3) \times (2n-3)}$ and the scale function $\tilde{s}(\mathbf{e})$ such that $\mathbf{e}_f \in \{\mathbf{e}|S\}$ and

$$J_v^*(\mathbf{e}_0, u(\tilde{s}(\mathbf{e}), \mathbf{e})) = \min_{\tilde{s} \in C(\mathbb{E})} J_v(\mathbf{e}_0, u(\tilde{s}(\mathbf{e}), \mathbf{e}), \tilde{s}(\mathbf{e})) \quad (18)$$

When $\Theta = s_c$, it is actually a matching of two fixed geometries without considering the scaling operation. When $\Theta = \tilde{s}(\mathbf{e})$, it turns to a matching of a geometry and a shape, which gives us more flexibility to optimize the geometry's DOS.

In the remaining context of the paper, we will discuss the optimization problem (16) and (18) respectively.

4. OPTIMAL FORMATIONS UNDER TIME-INVARIANT SHAPE SCALE

System with a constant scale s_c during the entire converging process is simple but typical. Instead of considering a determined final geometry at a randomly selected scale as discussed in Lemma 2.2, here given the initial relative realization \mathbf{e}_0 , we focus on finding an optimal s_c such that the formation system has the best cooperative performance.

When $\Theta = s_c$ and under the control law (15),

$$J_c(\mathbf{e}_0, u(\mathbf{e}, s_c), s_c) = \sum_{i=1}^n \frac{1}{8} (\|e_i(0)\|^2 - 2s_c \bar{s}_i)^2 \quad (19)$$

The partial derivative of J_c with respect to s_c is

$$\frac{\partial J_c}{\partial s_c} = \sum_{i=1}^n \frac{1}{2} (\|e_i\|^2 - 2s_c \bar{s}_i) \bar{s}_i \quad (20)$$

By letting (20) equal to zero, it immediately yields that the optimal solution s_c^* to problem (16) is

$$\sum_{i=1}^n (\|e_i(0)\|^2 - 2s_c^* \bar{s}_i) \bar{s}_i = 0 \quad (21)$$

Under Assumption 2.1, the analytical expression of the optimal scale is

$$s_c^* = \frac{\sum_{i=1}^n \|e_i(0)\|^2 \bar{s}_i}{2 \sum_{i=1}^n \bar{s}_i^2} \quad (22)$$

and it is obvious that $s_c^* \in \mathbb{R}^+$.

Rigidity corresponds to a unique realization of the graph only if the domain is small enough. For a globally unique realization, we have the idea of global rigidity [10] which tells that once the distances between any of the two neighboring agents are known, all the other distances for non-neighbors are uniquely determined. However, globally rigid graph is rigorous and there is no polynomial time algorithm to determine whether a graph is a globally rigid one or not. Meanwhile, its rigidity matrix is not a full rank matrix, which may brought some unexpected equilibriums in the rigidity matrix-based control laws. Thus we would like to focus ourselves on minimally rigid graph whose rigidity matrix is exactly of rank $2|V| - 3$.

Theorem 4.1

The formation system (14) over a minimally rigid graph converges to the largest invariant set

$$\mathcal{I}_e = \{\mathbf{e} \in \text{Im} \hat{H} : r(\mathbf{e}) - s_c^* \bar{S} = 0, \mathbf{z}_0 \in \Omega_\sigma\} \quad (23)$$

where

$$\begin{aligned} \Omega_\sigma(S) := \{ & \mathbf{e}_0 \in \mathbb{E} : \sum_{i=1}^n (r_i(\mathbf{e}_0) - r_i(\mathbf{e}))^2 + \\ & \sum_{l \neq m} \left(\frac{1}{2} \|z_{0l} - z_{0m}\|^2 - \frac{1}{2} \|z_l - z_m\|^2 \right)^2 < \sigma, \mathbf{e} \in \{\mathbf{e}|S\} \} \end{aligned} \quad (24)$$

for a sufficiently small σ if the control law is the one in (15). Furthermore, J_c^* is obtained when $s_c = s_c^*$ with s_c^* given in (22).

Proof

Similar to the proof of Lemma 2.2, the control law (15) for an arbitrary $s_c \in \mathbb{R}^+$ is a stabilization control law that guarantees the convergence to \mathcal{I}_e . The derivation of s_c^* indicates that (22) is the optimal solution to (16), which finishes the proof. \square

Remark 4.1

When the underlying graph G of the shape is a minimally rigid one, a shape S does not determine a geometry uniquely, and consequently $r(\mathbf{e}_f) = s_c^* \bar{S}$ does not ensure $\mathbf{e}_f \in \{\mathbf{e}|S\}$. However, when the initial geometry \mathbf{e}_0 of the formation system is restrained within a sufficiently small neighborhood $\Omega_\sigma(S)$ of a candidate geometry, $\dot{V}(\mathbf{e}) < 0$ guarantees the convergence to the desired shape.

The optimal scale s_c^* is, not surprisingly, uniquely determined by the initial geometry \mathbf{e}_0 and the desired shape S . It is the global optimum and is always positive with an upper bound when the formation is non-collinear.

In a formation system, when a set of agents equipped with sensors is deployed within a neighborhood of the desired shape specified by the shape vector $S(G)$, (22) helps us to decide the exact final geometry that requires a small range of transformations from \mathbf{e}_0 , and the control law drives the agents approach this optimal geometry.

5. FORMATION CONTROL UNDER TIME-VARYING SCALE FUNCTION

As mentioned previously, there are two kinds of strategies to find an appropriate shape scale one of which is to determine an optimal value a priori and set it constant during the entire process, as discussed in the previous section. Another more intelligent strategy is to consider the time-varying function \tilde{s} that adjusts the final scale online. This allows us to evaluate the resemblance of the geometry with respect to the desired shape more objective.

5.1. Formations with three agents

Triangular formations with three agents interconnected with one another are the most fundamental pattern in formation systems, and thus are embraced as the starting point in many literatures, as for example in [3, 27, 28]. Here we will also start with this simple and typical case and then further extend the results into multiple ($n > 3$) agents systems.

Under the fixed-structured control law (17), the dynamics of the formation system in the edge space is

$$\dot{\mathbf{e}} = \hat{H}u = -\hat{H}R(\mathbf{e})^T M(\mathbf{e})^T [r(\mathbf{e}) - \tilde{s}(\mathbf{e})\bar{S}] \quad (25)$$

The control law u is a function of both $\tilde{s}(\mathbf{e})$ and \mathbf{e} , and \mathbf{e} in $\tilde{s}(\mathbf{e})$ is also determined by u , which means u and $\tilde{s}(\mathbf{e})$ are highly coupled. This makes the solution to (18) becomes complex and the problem may not be solvable exactly.

Alternatively, we would like to seek for a function $\tilde{s}(\mathbf{e})$ for the following problem:

Problem 5.1

Find a trajectory for $\tilde{s} \in C(\mathbb{E})$, which is an explicit function of edge \mathbf{e} , such that

$$J_v(\mathbf{e}_0, u(\tilde{s}(\mathbf{e}), \mathbf{e}), \tilde{s}(\mathbf{e})) < J_c((\mathbf{e}_0), u(s_c, \mathbf{e}), s_c)$$

for all $s_c \in \mathbb{R}^+$.

Instead of concentrating on the complex optimization problem (18), we suggest to design an adjusting rule for the scale such that the formation system under the control law always exhibits better cooperative performance than the case with a constant scale.

Consider the equation

$$\frac{\partial J_v}{\partial \tilde{s}} \Big|_{\tilde{s}=\tilde{s}^*(\mathbf{e})} = 0 \quad (26)$$

which has the equivalent form of

$$\frac{\partial L}{\partial \tilde{s}} = 2[r(\mathbf{e})^T - \tilde{s}(\mathbf{e})\bar{S}^T]R(\mathbf{e})R(\mathbf{e})^T\bar{S} \quad (27)$$

where L is the loss function of J_v . By using the fact

$$e_i^T e_j = \|e_i\| \|e_j\| \cos\theta_{ij}$$

and the cosine law

$$\|e_i\| \|e_j\| \cos(\theta_{ij}) = \frac{1}{2}(\|e_i\|^2 + \|e_j\|^2 - \|e_k\|^2)$$

where e_i, e_j and e_k form an triangle, we obtain

$$\frac{\partial L}{\partial \tilde{s}} = 2[r(\mathbf{e}) - \tilde{s}(\mathbf{e})\bar{S}]^T \bar{D}r(\mathbf{e}) \quad (28)$$

where

$$\bar{D} = \begin{bmatrix} \bar{s}_2 + \bar{s}_3 - 4\bar{s}_1 & \bar{s}_2 - \bar{s}_3 & \bar{s}_3 - \bar{s}_2 \\ \bar{s}_1 - \bar{s}_3 & \bar{s}_1 + \bar{s}_3 - 4\bar{s}_2 & \bar{s}_3 - \bar{s}_1 \\ \bar{s}_1 - \bar{s}_2 & \bar{s}_2 - \bar{s}_1 & \bar{s}_1 + \bar{s}_2 - 4\bar{s}_3 \end{bmatrix} \quad (29)$$

If we let $\frac{\partial L}{\partial \tilde{s}} = 0$, a trajectory of $\tilde{s}(\mathbf{e})$ is then

$$\tilde{s}^*(\mathbf{e}) = \frac{r(\mathbf{e})^T \bar{D}r(\mathbf{e})}{\bar{S}^T \bar{D}r(\mathbf{e})} : \triangleq \frac{s_N}{s_D} \quad (30)$$

and next we prove that the cost function J_v with the scale (30) is consistently smaller than J_c .

Theorem 5.1

Given the same initial geometry \mathbf{e}_0 and the same desired shape S , the inequality

$$J_v(\mathbf{e}_0, u(\tilde{s}^*(\mathbf{e}), \mathbf{e}), \tilde{s}^*(\mathbf{e})) \leq J_c((\mathbf{e}_0), u(s_c, \mathbf{e}), s_c)$$

with \tilde{s}^* given in (30) always holds true for arbitrary $s_c \in \mathbb{R}^+$. The equality is satisfied if and only if $\mathbf{e}_0 \in \{\mathbf{e}|S\}$.

Proof

Substituting \tilde{s}^* into J_v , the difference of J_v and J_c is

$$\begin{aligned} & J_v - J_c \\ &= \int_0^\infty ((r - \tilde{s}^* \bar{S})^T R R^T (r - \tilde{s}^* \bar{S}) - (r - s_c \bar{S})^T R R^T (r - s_c \bar{S})) d\tau \\ &= \int_0^\infty [(\tilde{s}^{*2} - s_c^2) \bar{S}^T + 2(s_c - \tilde{s}^*) r^T] R R^T \bar{S} d\tau \\ &= \int_0^\infty (\tilde{s}^* - s_c)(\tilde{s}^* \bar{S}^T - r^T + s_c \bar{S}^T - r^T) R R^T \bar{S} d\tau \end{aligned} \quad (31)$$

Recall the characters of \tilde{s}^* ,

$$[r^T - \tilde{s}^* \bar{S}^T] R R^T \bar{S} = 0 \quad (32)$$

Based on the expression of \tilde{s}^* in (30),

$$\tilde{s}^* - s_c = \frac{(r^T - s_c \bar{S}^T) \bar{D} r}{\bar{S}^T \bar{D} r} \quad (33)$$

According to (32) and (33), equation (31) has the simplified form of

$$J_v - J_c = \int_0^\infty -\frac{1}{s_D} \bar{S}^T R R^T (r - s_c \bar{S}) (r^T - s_c \bar{S}^T) \bar{D} r d\tau$$

The positiveness of s_D is guaranteed according to the equality of

$$\bar{D} r = R R^T \bar{S}$$

which further yields

$$J_v - J_c = \int_0^\infty -\frac{1}{s_D} ((r^T - s_c \bar{S}^T) \bar{D} r)^2 d\tau \leq 0, \forall s_c > 0 \quad (34)$$

where equality holds if and only if $s_c \equiv \frac{\|e_i\|^2}{2s_i^2}, \forall i \in [1, 2, 3]$, i.e., $e_0 \in \{e|S\}$. \square

Even when $s_c = s_c^*$, the conclusion of J_v having a smaller value still holds true, which indicates that better cooperative performance is always observed on J_v .

Theorem 5.2

The triangular formation system (25) is exponentially stable and converges to the invariant set $\mathcal{I}_e = \{e \in \text{Im} \hat{H} : r(e) - \tilde{s}_f^* \bar{S} = 0\}$ if

$$M(e) = s_D^2 I_3 - s_D \bar{S} r(e)^T (\bar{D}^T + \bar{D}) + s_N \bar{S} \bar{S}^T \bar{D} \quad (35)$$

with parameters \bar{D} and s_D, s_N given in (29) and (30) respectively, and \tilde{s}_f^* is the stable value of the scale function $\tilde{s}(e)$.

Before giving the proof to Theorem 5.2, we first propose the following lemma

Lemma 5.1

Matrix $M(e), e \in \mathbb{E}$ in (35) is a singular matrix if and only if $r(e) = k \bar{S}$.

Proof

Let Q be the transformation matrix such that

$$Q \bar{S} = [\bar{s}_1 \quad 0 \quad 0]^T$$

Left multiplying matrix $M(e)$ by Q yields

$$\begin{aligned} QM(e) &= s_D^2 I Q - s_D \begin{bmatrix} \bar{s}_1 \\ 0 \\ 0 \end{bmatrix} r(e)^T (\bar{D}^T + \bar{D}) + s_N \begin{bmatrix} \bar{s}_1 \\ 0 \\ 0 \end{bmatrix} \bar{S}^T \bar{D} \\ &= \begin{bmatrix} s_D^2 - p_1 & -p_2 & -p_3 \\ -\frac{\bar{s}_2}{\bar{s}_1} s_D^2 & s_D^2 & 0 \\ -\frac{\bar{s}_3}{\bar{s}_1} s_D^2 & 0 & s_D^2 \end{bmatrix} \end{aligned} \quad (36)$$

where

$$p_i = s_D \bar{s}_1 \sum_{j=1}^3 r_j(e) (\bar{d}_{ij} + \bar{d}_{ji}) - s_N \bar{s}_1 \sum_{j=1}^3 \bar{s}_j \bar{d}_{ji}$$

and \bar{d}_{ij} is the elements of matrix \bar{D} . Matrix $M(\mathbf{e})$ is of full rank if and only if the diagonalize matrix $\text{diag}(m, s_D^2, s_D^2)$ with

$$m = s_D^2 - p_1 + \sum_{i=2}^3 \left(-\frac{\bar{s}_i}{\bar{s}_1} p_i \right)$$

consists of only nonzero diagonal entries, that is $m \neq 0$ or equivalently,

$$\sum_{i=1}^3 (\bar{s}_i p_i) \neq s_D^2 \bar{s}_1 \quad (37)$$

Recall (36), if we consider $\sum (\bar{s}_i p_i)$ as the inner product of the two vectors $\mathbf{p} = [p_1 \ p_2 \ p_3]^T$ and \bar{S} , we obtain

$$\sum_{i=1}^3 (\bar{s}_i p_i) = s_D \bar{s}_1 r^T (\bar{D}^T + \bar{D}) \bar{S} - s_N \bar{s}_1 \bar{S}^T \bar{D} \bar{S} \quad (38)$$

Substituting s_D and s_N given in (30) into (37) and by some trivial calculations, we conclude that the necessary and sufficient condition for $M(\mathbf{e})$ being a singular matrix is

$$\bar{S}^T \bar{D} r r^T \bar{D} \bar{S} = r^T \bar{D} r \bar{S}^T \bar{D} \bar{S} \quad (39)$$

which is satisfied if and only if $r(\mathbf{e}) = k \bar{S}$. \square

Proof of Theorem 5.2

Consider the positive semidefinite function

$$V(\mathbf{e}) = [r(\mathbf{e}) - \bar{s}^*(\mathbf{e}) \bar{S}]^T [r(\mathbf{e}) - \bar{s}^*(\mathbf{e}) \bar{S}] \quad (40)$$

and its partial derivative with respect to \mathbf{e}

$$\begin{aligned} \frac{\partial V}{\partial \mathbf{e}} &= 2 \frac{\partial [r^T - \bar{s}^* \bar{S}^T]}{\partial \mathbf{e}} [r - \bar{s}^* \bar{S}] \\ &= 2 [\Lambda(\mathbf{e}) - \frac{\partial \bar{s}^*}{\partial \mathbf{e}} \bar{S}^T] [r(\mathbf{e}) - \bar{s}(\mathbf{e}) \bar{S}] \end{aligned} \quad (41)$$

The partial derivative $\frac{\partial \bar{s}^*}{\partial \mathbf{e}}$ is calculated by first solving

$$\frac{\partial s_N}{\partial \mathbf{e}} = \Lambda(\mathbf{e}) (\bar{D}^T + \bar{D}) r(\mathbf{e})$$

and

$$\frac{\partial s_D}{\partial \mathbf{e}} = \Lambda(\mathbf{e}) \bar{D}^T \bar{S}$$

which then yield

$$\frac{\partial \bar{s}^*}{\partial \mathbf{e}} = \frac{s_D \Lambda(\mathbf{e}) (\bar{D}^T + \bar{D}) r(\mathbf{e}) - s_N \Lambda(\mathbf{e}) \bar{D}^T \bar{S}}{s_D^2} \triangleq N(\mathbf{e}) \quad (42)$$

Hence the derivative of $V(\mathbf{e})$ with respect to t is

$$\begin{aligned} \frac{d}{dt} V(\mathbf{e}) &= \left(\frac{\partial V(\mathbf{e})}{\partial \mathbf{e}} \right)^T \frac{d\mathbf{e}}{dt} \\ &= -2 [r(\mathbf{e}) - \bar{s}^*(\mathbf{e}) \bar{S}]^T [\Lambda(\mathbf{e}) - N(\mathbf{e}) \bar{S}^T]^T \hat{H} \hat{H}^T \Lambda(\mathbf{e}) M(\mathbf{e})^T [r(\mathbf{e}) - \bar{s}^*(\mathbf{e}) \bar{S}] \end{aligned} \quad (43)$$

When

$$M(\mathbf{e}) = s_D^2 I_3 - s_D \bar{S} r(\mathbf{e})^T (\bar{D}^T + \bar{D}) + s_N \bar{S} \bar{S}^T \bar{D} \quad (44)$$

the derivative of $V(\mathbf{e})$ in (43) is negatively semi-definite with the expression

$$\dot{V}(\mathbf{e}) = -\frac{2}{s_D^2} [r(\mathbf{e})^T - \bar{s}^*(\mathbf{e}) \bar{S}^T] M(\mathbf{e}) \Lambda(\mathbf{e})^T \hat{H} \hat{H}^T \Lambda(\mathbf{e}) M(\mathbf{e})^T [r(\mathbf{e}) - \bar{s}^*(\mathbf{e}) \bar{S}] \quad (45)$$

Indeed, $V(\mathbf{e})$ is a valid Lyapunov function candidate.

For the autonomous system when the derivative of the candidate Lyapunov function is negative semi-definite, the asymptotic stability is concluded based on the powerful invariant set theory.

For the negative semi-definite function $V(\mathbf{e})$, there is an invariant set

$$\Omega_\sigma = \{\mathbf{e} \in \text{Im}\hat{H} : V(\mathbf{e}) \leq c, c \in \mathbb{R}^+\}$$

The set of points in Ω_σ where $\dot{V}(\mathbf{e}) = 0$ satisfies both conditions

$$\bar{S}^T \bar{D}r(\mathbf{e}) \neq 0 \quad (46)$$

and

$$\hat{H}^T \Lambda(\mathbf{e}) M(\mathbf{e})^T [r(\mathbf{e}) - \tilde{s}^*(\mathbf{e})\bar{S}] = 0 \quad (47)$$

where condition (46) is always true under Assumption 2.1.

When the three agents are connected over the graph shown in Fig. 4(b), matrix $\hat{H}^T \Lambda(\mathbf{e}) \in \mathbb{R}^{6 \times 3}$ has rank 3 for all $\mathbf{e} = \hat{H}\mathbf{z} \in \mathbb{E}$.

In order to find the largest invariant set, the singularity of matrix $M(\mathbf{e})$ is crucial to the asymptotic stability. As pointed out by Lemma 5.1, $M(\mathbf{e})$ is a full rank matrix when $r(\mathbf{e}) \neq k\bar{S}$. Thus equation (47) is satisfied if and only if there exist \mathbf{e}_f such that $r(\mathbf{e}_f) = \tilde{s}^*(\mathbf{e}_f)\bar{S}$. Thus

$$\mathcal{I}_e = \{\mathbf{e} \in \text{Im}\hat{H} : r(\mathbf{e}) - \tilde{s}_f^* \bar{S} = 0\} \quad (48)$$

where $\tilde{s}_f^* = \tilde{s}^*(\mathbf{e}_f)$ is the largest invariant set for dynamic system (25).

If we let ϵ being the smallest eigenvalue of $RM M^T R^T$ during the entire convergence, the derivative of $V(\mathbf{e})$ is bounded by

$$\dot{V}(\mathbf{e}) \leq -\frac{2\epsilon}{\bar{s}_D^2} \|r(\mathbf{e}) - \tilde{s}(\mathbf{e})\bar{S}\|^2 \triangleq -\theta$$

which further yields $V(\mathbf{e}) \leq V(\mathbf{e}_0)e^{-\theta}$. According to some trivial calculations, we conclude that $\|r(\mathbf{e}) - \tilde{s}(\mathbf{e})\bar{S}\|$ exponentially converges to zero. \square

According to \mathcal{I}_e , once the formation system forms a geometry in $\{e|S\}$, it stays there from then on.

Equation (30) is a nonlinear map $\tilde{s} \in C(\mathbb{E}) : \mathbb{E} \rightarrow \mathbb{R}$ where given an assigned shape S , the initial geometry \mathbf{e}_0 in the nonlinear control law (30) uniquely determines the stable scale \tilde{s}_f^* . However, due to the nonlinearity, it is difficult to predict the final stable value \tilde{s}_f^* .

On the other hand, although the exact value of \tilde{s}_f^* is what we are seeking for, we would like to discuss the controllability of the algorithm when the scale is expected to converge to some arbitrary fixed value. In such a case, the problem is recast into a general formation control problem with a specified desired geometry, which is explored in quite a few works, e.g., [29]. However, we believe it is still necessary to make this extension so as to broaden the applications of the algorithm. This problem is covered in Subsection 5.3 after we extend the nonlinear control law to multiple ($n > 3$) agents case.

5.2. Formation with multiple agents

Some of related literatures concerning formation control were restricted to three agents [7, 20] and left the multiagents case as the future work. Extending algorithms into multiple agents case would have to deal with the complexity issue where the primary one is the selection of the underlying graph. A graph with three nodes connected with each other is a quite special case: it is a complete graph, a minimally rigid graph and a ring graph. During the exposition of Theorem 5.2, based on the cosine law, this particular property of the three nodes ensures the compact form of the partial derivative of the value function L . However, when the number of agents exceeds three, the cosine law dose not always applies.

In order to obtain the nonlinear control law as in three agents formations, an intuitive idea is to adopt triangle as the basic unit of the underlying graph. We define the *triangular complement* of a graph which would lead to some interesting and convenient results.

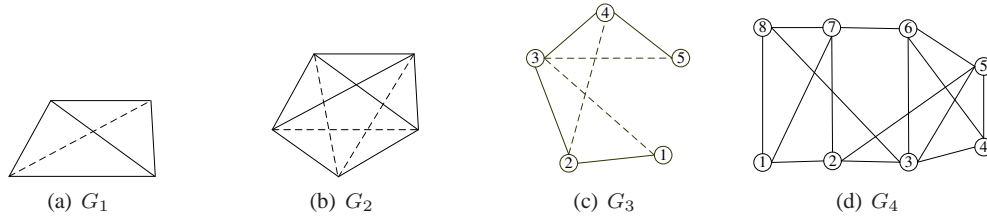


Figure 5. Graphs and their triangular complement graphs shown with dashed lines. G_1 and G_2 are minimally rigid graphs, G_3 is only a connected graph and G_4 is a globally rigid graph.

Definition 5.1

The *triangular complement* of a graph $G = (V, E)$ is a graph $G' = (V, E')$ with the same vertex set as G and node i are connected to node j in G' if and only if the minimal distance between i, j in G are two. The graph sum $G_\Delta = G + G'$ has vertex set V and edges $E_\Delta = E \cup E'$.

When the triangular complement graph is added to the minimally rigid graph, its edges are labeled from $|E| + 1$ to $|E| + |E'|$.

Corollary 5.1

The graph sum $G_\Delta = G + G'$ equals to G^2 .

For the definition of G^2 , please refer to, for example, [24, 30].

The triangular complement graph G' contains the third edges that constitute triangles with the neighboring edges in G , as shown in Fig. 5(a) and Fig. 5(b) where the solid lines are edges in G and the dashed lines belong to G' . However, the neighboring edges from G and G' respectively do not necessarily have a third edge in G_Δ that form a triangle, as shown in Fig. 5(c).

It is not necessarily true that G_Δ , or equivalently G^2 , being a complete graph even when G is minimally rigid or globally rigid, as for instance the situation in Fig. 5(d) where the length between node 4 and node 1 is greater than 2. That is the reason we name it triangular complement graph rather than the general complement graph as in [24].

The three edges e_i, e_j and e_γ in G_Δ that form a triangle is denoted by $\Delta_{ij\gamma}$. We have made the assumption in the preliminary that each agent has the knowledge of the coordinates of its neighbors, thus the agent that is adjacent to e_i and e_j in G is able to calculate the coordinates of the edges e_γ in G' , i.e., $e'_\gamma = e_i + e_j$ or $e'_\gamma = e_i - e_j$ for $\Delta_{ij\gamma}$.

For multiple agents case, the parallel form of matrix \bar{D} in (29) is denoted by $\hat{D}(G_\Delta) \in \mathbb{R}^{|E_\Delta| \times |E_\Delta|}$ with entries

$$\hat{d}_{ij} = \begin{cases} \sum_{k:k \in \mathcal{N}_e(i)} \bar{s}_k - 4\bar{s}_i & , i = j \\ \bar{s}_j - \bar{s}_\gamma & , \Delta_{ij\gamma}, i, j \in E, \gamma \in E \\ \bar{s}_j & , \Delta_{ij\gamma}, i, j \in E, \gamma \in E' \\ -\bar{s}_\gamma & , \Delta_{ij\gamma}, i, \gamma \in E, j \in E' \\ 0 & , \text{others} \end{cases}$$

If we define an expended shape vector $\hat{S} = [\bar{S}; \mathbf{0}] \in \mathbb{R}^{|E_\Delta|}$ and similarly $\hat{r}(\mathbf{e}) = [r(\mathbf{e}); r'(\mathbf{e})]$, $\hat{\mathbf{e}} = [\mathbf{e}; \mathbf{e}']$ where $r'(\mathbf{e})$, the norm of edges in G' , is calculated by the corresponding agent using local coordinates of the other two edges in G , and consequently, similar to (30) the trajectory of the scale function in terms of \mathbf{e} is

$$\hat{s}^*(\mathbf{e}) = \frac{\hat{r}(\mathbf{e})^T \hat{D} \hat{r}(\mathbf{e})}{\hat{S}^T \hat{D} \hat{r}(\mathbf{e})} \triangleq \frac{\hat{s}_N}{\hat{s}_D} \quad (49)$$

and

$$\frac{\partial \hat{s}_N}{\partial \mathbf{e}} = \hat{\Lambda}(\mathbf{e})(\hat{D} + \hat{D}^T) \hat{r}(\mathbf{e})$$

$$\frac{\partial \hat{s}_N}{\partial \mathbf{e}} = \hat{\Lambda}(\mathbf{e}) \hat{D}^T \hat{S}$$

where $\hat{\Lambda}(\mathbf{e}) = \frac{\partial \hat{r}(\mathbf{e})}{\partial \mathbf{e}} = [\Lambda(\mathbf{e}) \quad \Lambda'(\mathbf{e})] \in \mathbb{R}^{2|E| \times |E_\Delta|}$. This further yields

$$\hat{M}(\mathbf{e}) = \hat{s}_D^2 [I_{2n-3} \quad 0] - \hat{s}_D \hat{S} \hat{r}^T(\mathbf{e}) (\hat{D}^T + \hat{D}) + \hat{s}_N \hat{S} \hat{S}^T \hat{D} \quad (50)$$

where \hat{H} is still the oriented incidence matrix of G .

The derivative of the Lyapunov function (40) is then

$$\dot{V}(\mathbf{e}) = -\frac{2}{\hat{s}_D^2} [r(\mathbf{e})^T - \hat{s}(\mathbf{e}) \bar{S}^T] \hat{M}(\mathbf{e}) \hat{\Lambda}(\mathbf{e})^T \hat{H} \hat{H}^T \hat{\Lambda}(\mathbf{e}) \hat{M}(\mathbf{e})^T [r(\mathbf{e}) - \hat{s}(\mathbf{e}) \bar{S}] \quad (51)$$

Theorem 5.3

The formation system

$$\dot{\mathbf{e}} = -\hat{H} \hat{H}^T \hat{\Lambda}(\mathbf{e}) \hat{M}(\mathbf{e})^T [r(\mathbf{e}) - \hat{s}^*(\mathbf{e}) \bar{S}], \mathbf{e}_0 \in \Omega_\sigma \quad (52)$$

over a minimally rigid graph is exponentially stable and converges to the largest invariant set \mathcal{I}_e in (48) if $\hat{s}^*(\mathbf{e})$ and \hat{M} are given in (49) and (50) respectively.

PROOF

The first part of the stability proof is identical to that of three agents situation. When $n \geq 4$, for a minimally rigid graph we have the similar results that $\text{rank} \hat{M}(\mathbf{e}) = 2n - 3$ if and only if $r(\mathbf{e}) = k \bar{S}$, and it is also trivial that $\hat{H}^T \Lambda(\mathbf{e}) \hat{M}^T$ is of rank $2|V| - 3$. Following the proof of Theorem 5.2 we conclude that the largest invariant set is \mathcal{I}_e in (48), which indicates that the formation system converges to the desired shape at some scale \hat{s}_f for a sufficiently small σ .

The proof of exponential convergence is consistent to that of three agents case and is omitted here. \square

Remark 5.1

When we considers only three agents in a formation system, the underlying graph is a globally rigid one and a minimally rigid one simultaneously, thus the requirements on the initial realization is relaxed. However for system with up to four agents, this privilege dose not holds true. Thus it is required that the initial geometry $\mathbf{e}_0 \in \Omega_\sigma$, and Remark 4.1 applies.

Remark 5.2

If we look at $[r(\mathbf{e}) - \hat{s}^*(\mathbf{e}) \bar{S}]$ in the control law, we require only a local coordinate for each node rather than a global one. The reason is that in the control law, we only concern with the relative distance between two agents, as represented by vector $r(\mathbf{e})$. On the other hand, in order to calculate $r'(\mathbf{e})$, local coordinates of two neighboring edges would be enough as well. However, for the rigidity matrix $\hat{R}(\mathbf{e}) = \hat{\Lambda}(\mathbf{e})^T \hat{H}$, it requires the relative coordinates in a common reference frame. So for convenience, we assign a global coordinate for the formation system.

With the time-varying scale function \hat{s}^* , the desired geometry $\hat{s}(\mathbf{e}_f)$ is adjusted according to the current geometry. Equation (49) is a nonlinear mapping $\hat{s} \in C(\mathbb{E}) : \mathbb{E} \rightarrow \mathbb{R}$ where the initial condition \mathbf{e}_0 uniquely determines the stable scale \hat{s}_f^* for the prescribed shape S . The scale function \hat{s}^* would lead to a bounded scale and ensure a relatively small cost value. This performance is observed in the experiments in Section 7.

5.3. Controllability of the multi-agent formation system

The aforementioned nonlinear functions \tilde{s}^* and \hat{s}^* put us in a blind position about the exact side lengths when agents get stabilized, and thus restricts the applications of the algorithms. For instance, in the task of payload transport, the desired geometry is constrained within a certain area determined by the cargo. Formation that shrinks to some geometry with a relatively small scale around the center of gravity may result in a sensitive balance system and a sparse formation where agents locate at the edge of the cargo may easily failed.

In order to drive the formation system to converge to an assigned geometry that belongs to $\{\mathbf{e}|S\}$, we add an additional control gain Π to the nonlinear control law

$$\dot{\mathbf{z}} = -\Pi\hat{H}^T\hat{\Lambda}(\bar{\mathbf{e}})\hat{M}(\bar{\mathbf{e}})^T[r(\bar{\mathbf{e}}) - \hat{s}^*(\bar{\mathbf{e}})\bar{S}] \quad (53)$$

where $\bar{\mathbf{e}} \in \mathbb{E}$, $\bar{\mathbf{z}} \in \mathbb{Z}$ and $\Pi = \text{diag}(a_1, a_2, \dots, a_{2n})$. The edge and the state of each agent that evolve along (53) are denoted by $\bar{\mathbf{e}}$ and $\bar{\mathbf{z}}$ respectively.

The weight factor a_i adjusts the convergence rate of each edge and thus tunes the stable value $\bar{\mathbf{e}}_f$ and $\hat{s}^*(\bar{\mathbf{e}}_f)$, and we will prove that the formation system under control law (53) is controllable.

Theorem 5.4

Given a desired geometry $\bar{\mathbf{e}}_f$ in $\{\mathbf{e}|S\}$, there exists Π satisfying $a_i > 0, \forall i \in [1, 2n]$ in (53) such that a formation system over a minimally rigid underlying graph exponentially converges to $\bar{\mathbf{e}}_f$ given that $\bar{\mathbf{e}}_0 \in \Omega_\sigma$.

PROOF

We prove the theorem by finding the appropriate Π with respect to λ such that $r(\bar{\mathbf{e}}) \rightarrow \lambda\bar{S}$. The procedure could be carried out by taking the original system (25) as a reference system.

Assume $r(\mathbf{e}) \rightarrow \hat{s}^*(\mathbf{e}_f)\bar{S}$ and $r(\bar{\mathbf{e}}) \rightarrow \hat{s}^*(\bar{\mathbf{e}}_f)\bar{S}$ where $\hat{s}^*(\bar{\mathbf{e}}_f) = \lambda$, and $\mathbf{e}_0 = \bar{\mathbf{e}}_0$. Let $k = \hat{s}^*(\bar{\mathbf{e}}_f)/\hat{s}^*(\mathbf{e}_f)$.

Apparently, $\dot{\bar{\mathbf{e}}} = \hat{H}\Pi\dot{\mathbf{z}}$. Integrating on each side of the equation yields

$$\bar{\mathbf{e}}_f - \bar{\mathbf{e}}_0 = \hat{H}\Pi(\mathbf{z}_f - \mathbf{z}_0) \quad (54)$$

The condition that $r(\bar{\mathbf{e}}) \rightarrow k\hat{s}^*\bar{S}$ is equivalent to, for each edge vector e_i ,

$$\bar{\mathbf{e}}_{f_i} = kR(\theta)\mathbf{e}_{f_i} + \mathbf{p}_i \quad (55)$$

with vector $\mathbf{p} = [\mathbf{p}_i] \in \mathbb{E}$. Substituting (55) into (54) we obtain

$$\hat{H}\Pi(\mathbf{z}_f - \mathbf{z}_0) = k\hat{R}(\theta)\hat{H}\mathbf{z}_f - \mathbf{e}_0 + \mathbf{p} \quad (56)$$

where $\hat{R}(\theta)$ is a block diagonal matrix with 2×2 identical diagonals $R(\theta)$. In order to analysis the solution of a_i , (56) could be rewritten into a standard linear matrix equation with respect to a_i

$$\hat{H}\Lambda(\Delta\mathbf{z}) \begin{bmatrix} a_1 \\ a_2 \\ \vdots \\ a_{2n} \end{bmatrix} = k\hat{R}(\theta)\hat{H}\mathbf{z}_f - \mathbf{e}_0 + \mathbf{p} \\ \triangleq kO(\mathbf{z}_f) - \mathbf{e}_0 + \mathbf{p} \quad (57)$$

where $\Lambda(\Delta\mathbf{z}) = \text{diag}(\mathbf{z}_{f_i} - \mathbf{z}_{0_i})$.

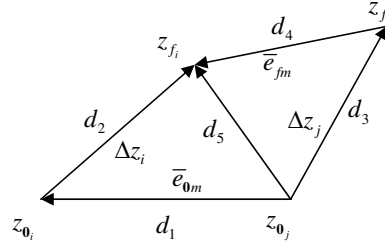
Noting that for a minimally rigid graph, $\text{rank}(\hat{H}) = 2n - 2$, i.e. $\dim(\ker(\hat{H})) = 2$. On the other hand, $\text{rank}(O) = 2(2n - 3)$. We can always find a set of positive numbers a_i in (57) by choosing appropriate \mathbf{p} such that the number of the nonzero entries of the right hand side vector is less than $2n - 2$.

With the positive control gain Π , the stability of the formation system under the advanced control law (53) could be proved along the same line as Theorem 5.3, which finishes the proof. \square

Remark 5.3

In order to ensure the convergence to the desired shape, restrictions on the initial conditions, i.e., Remark 4.1 remain applies.

Recall Theorem 5.1, under the endpoint constraints $\hat{s}_f^* = \lambda$, the control law (53) still inherits the suboptimality of $J_v|_{\Theta=\hat{s}^*}$ with respect to J_c .

Figure 6. Geometric analysis of the control gain Π

The existence of the positive gain Π could also be validated by the geometric representation of (57). Condition (57) is satisfied if and only if for all $m \in |E_{\Delta}|$,

$$\begin{bmatrix} a_{2i-1} & 0 \\ 0 & a_{2i} \end{bmatrix} \Delta z_i - \begin{bmatrix} a_{2j-1} & 0 \\ 0 & a_{2j} \end{bmatrix} \Delta z_j = \bar{e}_{f_m} - \bar{e}_{0_m} \quad (58)$$

where $\Delta z_i = z_{f_i} - z_{0_i}$. Equation (58) determines the adjacency of vectors in Fig. 6. According to the triangle inequality,

$$d_2 - d_1 - d_3 \leq d_4 \leq d_1 + d_2 + d_3$$

where $d_1 = \|e_{0_1}\|$, $d_2 = \|l_i(z_{f_i} - z_{0_i})\|$, $d_3 = \|l_j(z_{f_j} - z_{0_j})\|$, $d_4 = \lambda s_m$ and $l_i = \text{diag}(a_{2i-1}, a_{2i})$. By positioning vector \bar{e}_{f_m} on the upper right side of \bar{e}_{0_m} , it is always guaranteed that $l_i > 0, \forall i \in [1, n]$.

The discussion on the controllability allows the algorithms to be applied to situation that requires the switching of the geometry's scale during the mission. For example when underwater vehicles are mapping out oceanbed[31], the scale of the formation is adjusted online to decrease the interpolation error.

As stated before, this special problem we considered above falls into to the general formation control category where the optimization is carried out under the constraint of a fixed geometry. However those existing results mainly focus purely on minimal energy expenditure[29] rather than the geometrical performance during the process. In our research the cost function is carefully designed so as to have the group of agents exhibits prominent geometrical performance during convergence.

In reality, the final scale \hat{s}_f^* should be restrained within an interval. Generally, the upper bound could be the communication range of agents, and for lower bound, the collisions of agents should be taken into account.

In this section, motivated by the fact that a scale being adjusted online may result in better cooperative performance, we found a time-varying scale function in terms of the edge vector e that further reduces the global minimum of system with a constant scale. By introducing the triangular complement graph, we derived a compact form of the nonlinear control law for multiple agents. With the additional control gain, the nonlinear control law is also applicative to general formation control problems with fixed final geometry.

6. GEOMETRICAL PERFORMANCE IN SENSOR-TARGET LOCALIZATIONS

The localization of target in sensor networks is always carried out by a fleet of three UAVs in triangle. Each of the UAVs is equipped with sensors that gather information of the target based on bearing measurements[32], range measurements[33] or scan measurements[34]. A lot of literatures are devoted to the exploit of the sensors positioning strategy as it is strongly related to the localization performance. Based on Fisher information matrix, the pioneering work demonstrated

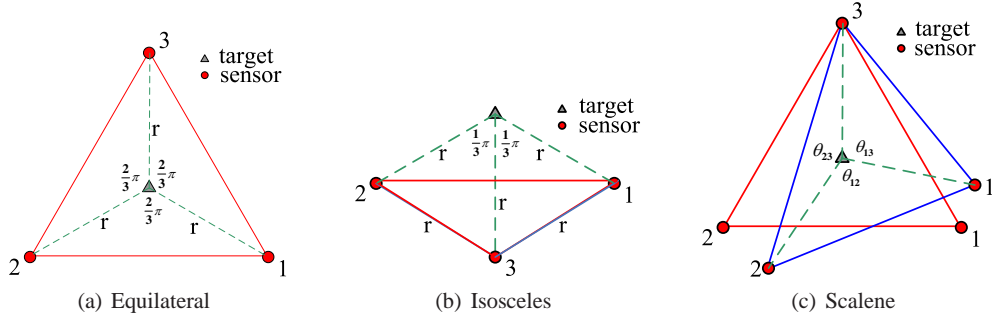


Figure 7. Optimal triangles for bearing-only sensor-target localization and a normal triangle as shown in color blue

in [16] proved that sensors in a equilateral triangle provide the minimal variance estimation of the target.

Consider the special scenario where sensors (or UAVs that are equipped with sensors) are deployed on a circle of radius r around the target. When r is sufficiently large such that the distances from the target to the three sensors could be considered as being constant during the entire formation attainment process, one of the main results in [16] could be restated specifically as

Lemma 6.1

Consider angle-based bearing-only localization with three sensors. Assume the distance between sensor i and the target, denoted by r_i , satisfies $r_i \equiv r, \forall i = 1, 2, 3$. Then the variance estimation of the target position is minimized if the triangle formed by the three sensors satisfies

$$\begin{aligned}\theta_{12} = \theta_{13} &= \frac{1}{2} \arccos\left(-\frac{1}{2}\right) \\ \theta_{23} &= 2\pi - \theta_{12} - \theta_{13}\end{aligned}\quad (59)$$

where $\theta_{ij} \in [0, \pi]$ is the angle subtended at the target by two sensors i and j . Moreover, reflecting a sensor about the target position does not affects the optimality of the geometry.

When the distances between sensors and the target are congruent, the optimal geometries generated from (59) have only angles constrains and are divided into two subsets where geometries in each of them are similar ones. Examples of the optimal geometries in the two subsets are shown in Fig. 7(a) and Fig. 7(b) respectively. For situations in Fig. 7(a), any equilateral triangles with the target locate at the geometry center are considered to be the optimal deployment of sensors while irrespective of their exact sizes. Thus here we focus on this optimal case to exploit the relationship between the variance estimation of the target and the resemblance of a geometry with respect to the equilateral triangle.

Consider a target that lies close to an equilateral triangle whose angles are denoted by θ'_{12} , θ'_{13} and θ'_{23} respectively, as shown in Fig. 7(c). Without lose of generality, assume $\theta'_{23} > \theta'_{12} > \theta'_{13}$. Then for simplicity, the difference between a shape with respect to the equilateral triangle could be measured by

$$\delta^{-1} = \Delta_1 + \Delta_2 := |\theta'_{12} - \theta'_{13}| + |\theta'_{23} - \theta'_{12}| \quad (60)$$

A geometry with a larger δ has a higher degree of similarity to a equilateral triangle.

The variance estimation of the target position measured by the sensors are evaluated by the determinant of the Fisher information matrix $I(\theta)$. Under constraints (59), the determinant of $I(\theta)$ achieves its maximum of [16]

$$\det(I(\theta^*)) = \frac{1}{\sigma_\theta^4} \sum \frac{3 \sin^2 \frac{2}{3}\pi}{r^4} = \frac{9}{4r^4\sigma^4} \quad (61)$$

where σ is the congruent error variance of sensors.

For a scalene triangle with angles θ'_{ij} , the difference between the determinant values of $\det(I(\theta^*))$ and $\det(I(\theta'))$ is

$$\Delta = \frac{1}{r^4 \sigma^4} (\cos \theta'_{23} \cos(\theta'_{12} - \theta'_{13}) + \cos \theta'_{13} \cos(\theta'_{12} - \theta'_{23}) + \cos \theta'_{12} (\theta'_{23} - \theta'_{13})) \quad (62)$$

The following theorem shows how δ in (60) affects the localization accuracy.

Theorem 6.1

The following two conditions are true if $\theta'_{13} > \frac{\pi}{2}$.

- i). when Δ_2 is constant, Δ increases as Δ_1 increases;
- ii). when Δ_1 is constant, Δ increases as Δ_2 increases.

PROOF

$$\frac{\partial \Delta}{\partial \Delta_1} = \frac{2}{3} (2 \sin \frac{2}{3} (2\pi - \Delta_2 - 2\Delta_1) - \sin \frac{2}{3} (2\pi - \Delta_2 + \Delta_1)) - \sin \frac{2}{3} (2\pi + 2\Delta_2 + \Delta_1) \quad (63)$$

Similarly,

$$\frac{\partial \Delta}{\partial \Delta_2} = \frac{2}{3} (\sin \frac{2}{3} (2\pi - \Delta_2 + \Delta_1) + \sin \frac{2}{3} (2\pi - \Delta_2 - 2\Delta_1)) - 2 \sin \frac{2}{3} (2\pi + 2\Delta_2 + \Delta_1) \quad (64)$$

The sufficient conditions for $\frac{\partial \Delta}{\partial \Delta_1} > 0$ and $\frac{\partial \Delta}{\partial \Delta_2} > 0$ are

$$\Delta_2 + 2\Delta_1 < \frac{\pi}{2} \quad (65)$$

when $\Delta_1 > \Delta_2$,

$$0 < \Delta_2 - \Delta_1 < \frac{\pi}{2}, 2\Delta_1 + \Delta_2 < \frac{\pi}{2} \quad (66)$$

when $\Delta_1 < \Delta_2$, and $\Delta < \pi/6$ when $\Delta_1 = \Delta_2 = \Delta$. Thus irrespective of the relationship between Δ_1 and Δ_2 , $\frac{\partial \Delta}{\partial \Delta_1} > 0$ and $\frac{\partial \Delta}{\partial \Delta_2} > 0$ are sufficiently true if

$$0 < \Delta_2 - \Delta_1 < \frac{\pi}{2}$$

and

$$0 < 2\Delta_1 + \Delta_2 < \frac{\pi}{2}.$$

or equivalently,

$$\begin{aligned} \theta'_{23} + \theta'_{13} - 2\theta'_{12} &< \frac{\pi}{2} \\ 2\theta'_{23} - \theta'_{12} - \theta'_{13} &< \frac{\pi}{2} \end{aligned} \quad (67)$$

Thus under the assumption that $\theta'_{23} > \theta'_{12} > \theta'_{13}$, inequality

$$\theta'_{13} > \frac{\pi}{2}$$

is the sufficient condition to *i*) and *ii*). □

It can be proved with some trivial calculation that the DOS defined in (9) is positively monotonic to δ^{-1} , that is

Corollary 6.1

In bearing-only sensor-target localization with three sensors, assume the smallest angle that is subtended by two sensors at the target is greater than $\frac{\pi}{2}$. Then the three sensors provides better estimation of the target location if the DOS of the triangle to the equilateral triangle is higher.

Generally in UAV localizations, the three UAVs are set off from certain locations and are commanded to fly towards the destination separately. Localization of the target is carried out after they attain the desired geometry at the destination. However, instead of relying completely on the final attainment of the formation, according to Theorem 6.1, we suggest that if we can take the formation performance $J(\mathbf{e}_0, u, \Theta)$ into account *during* attainment, the geometries that are resemble to the optimal one can provide pre-measurements of the target location before arriving at the destination. Strategies could be made based on those forecasted data and the executing time could be cut down if the localization is not expected to be highly accurate.

Simulations are given at the end of Section 7 to show the improvement of the localization capability when the control law (17) with $\tilde{s}(\mathbf{e}) = \tilde{s}^*(\mathbf{e})$ is applied.

7. EXAMPLES AND SIMULATIONS

In order to validate the effectiveness and the system performance of the proposed nonlinear control laws and the superiority of the time-varying scale function, we compare system performance under the control laws introduced in Section 4 and Section 5.

For multiple agents, the underlying minimally rigid graph is not unique, which inspires us to explore how the topology affects the system performance. Recall that a triangular complement graph is defined when applying the control law to multiple agents, we suggest to categorize the minimally rigid graphs by the number of edges in their triangular complement graphs, and then analysis their corresponding performance.

Apart from comparing the cost values, we also observe the maximal and total distance agents travel. These might be important in certain scenarios although they are not our primary concerns in this research. However, this observation could be a starting point for the future work.

The cooperative performance and its relationship to the cost function is illustrated in an intuitive way to further demonstrate the feature of the cost function.

Conclusions and conjectures are drawn from the results on how the underlying topology and the initial realizations are related to the cooperative performance.

7.1. The scales of geometries and the performance

We show the energy saving of a formation system under the optimal invariant scale s_c^* and compare it with other invariant scales. Consider a formation system consists of four agents that are initialized at $\mathbf{z}_0 = [0; 0; 1; 0; 1; 2; 0; 2]$ over a minimally rigid graph G_a in Fig. 8(a). The desired shape corresponds to G_a is measured by $\bar{S} = [3; 3; 3; 2; 3]$. The time-invariant scales are scanned from 0.1 to 0.9 at step length 0.1 and the cost value J_c at different s_c are shown in Fig. 9(a). The data when $s_c = 0.1, 0.3$ and 0.9 are recorded in Table I. According to Fig. 9(a), the optimal time-invariant scale is $s_c^* = 0.5$ which is exactly the value calculated from (22), and the optimal cost value is $J_c^* = 2.1249$, as shown in Table I. The formations when $s = 0.5$ and $s = 0.9$ are shown in Fig. 9(b) and Fig. 9(c) respectively. This verifies our conclusion that (22) helps to pick up the optimal geometry in $\{\mathbf{e}|S\}$ and the control law (15) drives the formation system attain this geometry when initialized within a qualified neighborhood.

Moreover, we compare the differences between the cost functions J_c and J_v . The data in Table I infers that when converge to the same geometry, formation system with time-varying scale $\hat{s}^*(\mathbf{e})$ has less cost value than system with constant scale, which is measured by 1.7402 and 2.1249 respectively. This result verifies the advantages that are brought by $\hat{s}^*(\mathbf{e})$ in the nonlinear formation system.

We further observe the distance each agent travels during the process and record the data in the table. According to the data, the total distance the four agents travel has a relatively smaller value of 1.8422 when the scale is a time-varying function. On the other hand, if we look at the maximal distance of the four agents travel at different scales (as distinguished by underlines), agent 4 has the smallest traveling distance of 0.6003 when $s_c \equiv 0.5$.



Figure 8. Two different graphs with the same number of triangular complement edges

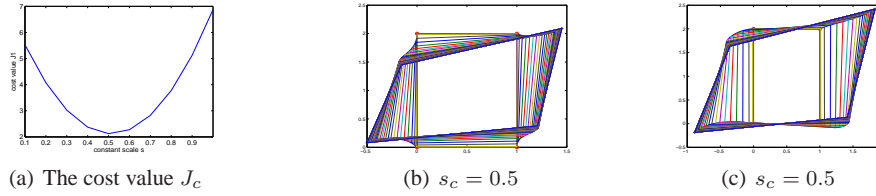


Figure 9. Formation system under time-invariant scale

 Table I. Time-varying VS. Time-invariant scale under G_a

Initial Conditions $n = 4; \mathbf{z}_0 = [0; 0; 1; 0; 1; 2; 0; 2]; S = [3; 3; 3; 2; 3]$				
	s_c	J	L : Length of each route	$Sum(L)$
Invariant scale	0.1	5.5227	[0.5167 0.7831 0.4686 0.8318]	2.6002
	0.3	2.8944	[0.4306 0.5534 0.3297 0.6700]	1.9837
	0.9	5.1248	[0.9559 0.6111 0.9346 0.6331]	3.1347
	0.5	2.1249	[0.5775 0.4608 0.4933 0.6003]	2.1319
Varying scale	0.3	1.7402	[0.3898 0.5190 0.2814 0.6519]	1.8422

7.2. The Topology, the initial geometry and the cooperative performance

In the category of minimally rigid graphs, according to their triangular complement graphs, they could be divided into different subsets where graphs G that belong to the same subset have the same number of edges in G^2 , i.e., $|E'|$ of G' are identical. In this subsection, parallel experiments are carried out over graphs that are within one subset and between different subsets respectively.

For comparison, the four agents in the previous experiment are assigned with another minimally rigid graph shown in Fig. 8(b), which also has one edge in its triangular complement graph. The initial condition and the desired shape are supposed to be the same as that of G_a . Note that for different underlying graphs, the shape vector S differs as well. When applying the nonlinear control law (52) on systems interconnected over G_b , the scale converges to 0.3563. The cost value of the system over G_b is 4.2120, compared to that of 1.7402 for G_a . The data is recorded in Table II. Fig. 10 demonstrates the geometry of the agents system and the trajectory of the scale $\hat{s}^*(e)$. The circles represent their initial positions and the bold blue lines are their final realization.

Apart from the cost value, Table II also shows that the total distance all agents travel is 1.8766 for graph G_b , which is larger than that of G_a .

Topology affects the system performance in terms of cost value and the sum of lengths each node travel. According to the experimental results, G_a should be considered as being better than G_b both in cooperative performance and the total traveling distance. Although the sub-optimization problem we discussed throughout the paper depends highly on the initial conditions, the fact that G_a outperforms G_b stays true for all cases we tested with a large number of different initial realizations.

We further investigate another situation where two underlying graphs have different numbers of triangular complement edges. We consider six agents over four different minimally rigid graphs, as shown in Fig. 11. The trajectories of the formation system are shown in Fig. 12 with experimental

Table II. Systems over different underlying graphs with identical $|E'|$

	\hat{s}_f^*	J_v	L : Length of each route	$Sum(L)$
G_a	0.3159	1.7402	[0.3898 0.5190 0.2814 <u>0.6519</u>]	1.8422
G_b	0.3563	4.2120	[0.3711 0.5013 0.3705 <u>0.6338</u>]	1.8766

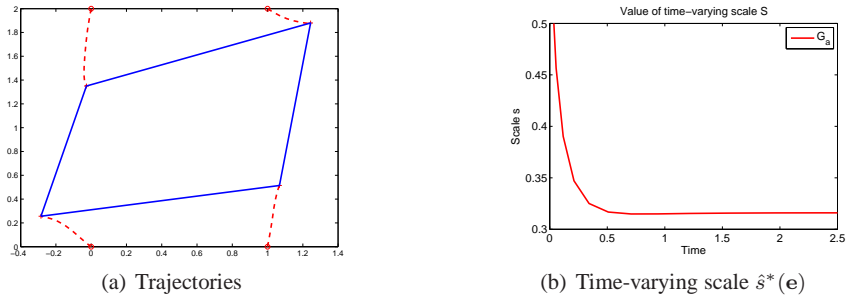


Figure 10. Four agents formations and the scale $\hat{s}^*(e)$ over G_a

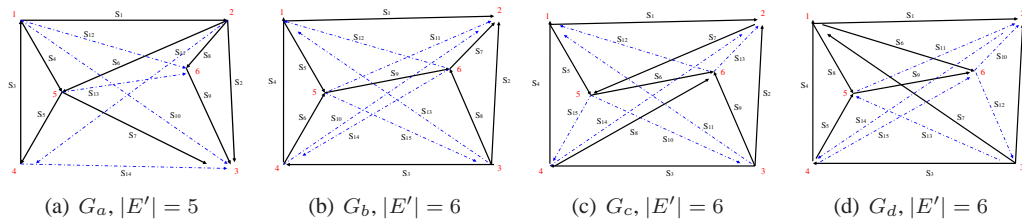


Figure 11. Four different graphs with different number of triangular complement edges. The bold lines indicate the minimally rigid graphs, and dashed lines are their triangular complement edges

results recorded in Table III. The curves for the time-varying scale $\hat{s}^*(e)$ over the four graphs are demonstrated in Fig. 13.

A significant difference between G_a and the other three graphs is that G_a only requires 5 additional edges for its triangular complement graph while the number is 6 for the other three. This interesting property explains the differences of the cost values and total traveling distances in Table III. Even with different initial realizations z_0 and z'_0 that differs on the position of agent 4, the cost value under G_a is consistently smaller than that of the other three graphs, as shown in the upper part and the bottom part of the table respectively.

The data corresponding to the four graphs infer the possibility that the system whose underlying graph having a smaller number of triangular complement edges, such as G_a , may exhibit a better cooperative performance than the one with more triangular complement edges, such as G_b , G_c and G_d .

On the other hand, the maximal distance the six agents travel, as highlighted with underlines in the table, also proves the superiority of graph G_a over the others. The smallest maximal distance agents travel is observed in G_a , which helps to prevent the overwhelming of a single agent. This is again only a conjecture from the current experiment without theoretical proofs, which is an ongoing work to this research.

The DOSs of the four graphs G_a , G_b , G_c and G_d to the desired shape are shown in Fig. 14. The solid line, which corresponds to graph G_a , has both a fast convergence speed and stay in a high DOS during the process. Although system over G_c achieved the desired shape as fast as the one over G_a did, its geometric distance to the desired shape during convergence was much larger.

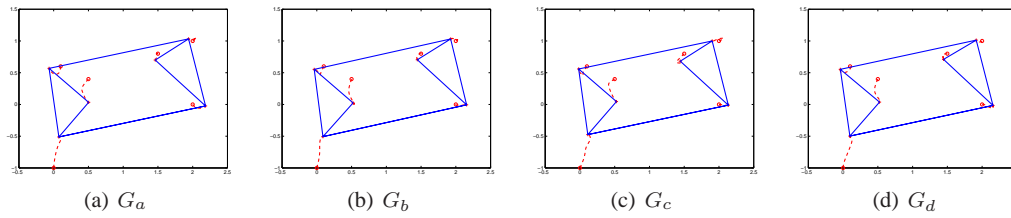


Figure 12. Trajectories of six agents interconnected over different graphs

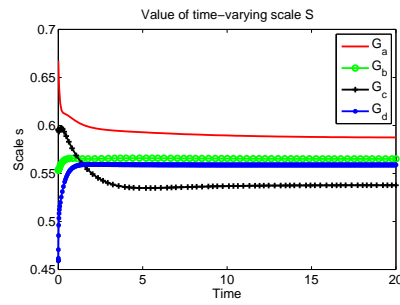


Figure 13. Scale $\hat{s}^*(e)$ over the four graphs

Table III. Systems over different underlying graphs where $|E^l|$ differs

$n = 6; S(G_a) = [3.6; 1; 1.01; 0.52; 0.41; 2.61; 2.41; 0.29; 0.89];$ $\bar{S}(G_b) = [3.6; 1; 4; 1.01; 0.52; 0.41; 0.29; 0.89; 1.16]$ $\bar{S}(G_c) = [3.6; 1; 4; 1.01; 0.52; 1.16; 2.61; 2.89; 0.89];$ $\bar{S}(G_d) = [3.6; 1; 4; 1.01; 0.41; 2; 4.6; 0.52; 1.16]$				
$\mathbf{z}_0 = [0.1; 0.6; 2; 1; 2; 0; 0; -1; 0.5; 0.4; 1.5; 0.8];$				
	\hat{s}_f^*	J_v	L : Length of each route	$Sum(L)$
G_a	0.5873	0.6918	[0.3143 0.2128 0.2214 <u>0.5202</u> 0.4290 0.1411]	1.8388
G_b	0.5652	0.7724	[0.2805 0.1532 0.1737 <u>0.5289</u> 0.4500 0.1488]	1.7351
G_c	0.5369	0.9152	[0.2900 0.2767 0.1799 <u>0.5628</u> 0.4139 0.2713]	1.9946
G_d	0.5589	0.9169	[0.2407 0.1185 0.2152 <u>0.5305</u> 0.3916 0.1189]	1.6154
$\mathbf{z}'_0 = [0.1; 0.6; 2; 1; 2; 0; -1; 0; 0.5; 0.4; 1.5; 0.8];$				
	\hat{s}_f^*	J_v	L : Length of each route	$Sum(L)$
G_a	0.6105	1.0284	[0.5100 0.2428 0.1906 <u>0.7621</u> 0.3985 0.1467]	2.2507
G_b	0.5838	1.5533	[0.6338 0.4744 0.5584 <u>0.7953</u> 0.3977 0.3489]	3.2086
G_c	0.5421	1.7603	[0.4980 0.5902 0.4058 <u>0.8065</u> 0.4816 0.4097]	3.1918
G_d	0.5570	2.4951	[0.5947 0.2069 0.4649 <u>0.8142</u> 0.3718 0.4263]	2.8788

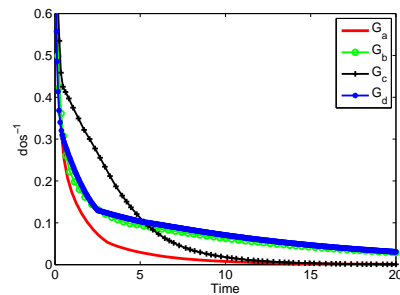
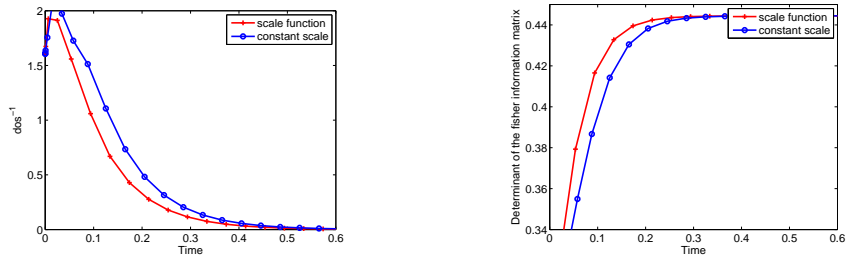


Figure 14. The inverse of the geometry's DOS at time t



(a) The inverse of the triangles DOS to the equilateral one (b) Determinant of the Fisher information matrix

Figure 15. Formation control in bearing-only sensor-target localization

7.3. Geometries in sensor-target localization

A triangle that has a higher DOS to the equilateral one could provide better estimation of the target location, as discussed in Section 6.

We consider three agents initialized at $\mathbf{z}_0 = [0; 0; 3; 1.5; 4; 0]$. The desired shape is a equilateral triangle, which is one of the optimal shapes in bearing-only sensor-target localization. The specialty of equilateral triangle For systems with the time-varying scale function and with a constant scale respectively, the geometries' DOS during the process are shown in Fig. 15(a).

The determinant of the Fisher information matrix during the process is calculated in Fig. 15(b). The system with a constant scale has consistently smaller degree of similarity to the equilateral triangle, and also smaller determinant value, which indicates the variance estimation is relatively worse. This validates the conclusion of Corollary 6.1.

8. CONCLUSIONS AND FUTURE WORKS

For a formation system with a flexible scale but under shape constraints, we discussed the strategies of choosing the desired geometries' scale so as to achieve better cooperative performance. In order to ensure the exponential stability of the system over a minimally rigid graph, fixed-structured nonlinear control laws on the edges and the scale were considered, where two types of scale design methods were proposed, namely the time-invariant scale and the time-varying scale function. It was proved that a system with the time-varying scale function could further reduce the minimum of the cost value when the scale is constant. By defining a triangular complement graph, the algorithm also applied to the multiple agents case. The controllability of the formation system was also discussed by adjusting the convergence rate of each edge with respect to the reference system.

These results were validated on various simulations where we compared the cost values of systems with constant scale and the time-varying scale function respectively. The experimental results also inferred the possibility that the underlying topology with a smaller number of triangular complement edges may always cost less during convergence and thus may have better cooperative performance. Theoretical proof to this conjecture is still undergoing. Moreover, we also applied the control laws in sensor-target localization to show the prominent features of the nonlinear formation system we designed.

The nonlinear dynamics (52) is a centralized control law as $\hat{\mathbf{s}}^*(\mathbf{e})$ contains states information of every agent in the system rather than local information. Decentralized/distributed algorithms should be considered in the future so as to meet the scalability requirements. Moreover, further research should focus on eliminating the restriction on the minimally rigid underlying graph.

ACKNOWLEDGEMENT

The authors would like to thank Professor Brian Anderson for the insightful comments and discussions, which have significantly improved the presentation of this work.

REFERENCES

1. Anderson BDO, Yu C, Dasgupta S, Morse AS. Control of a three-coleader formation in the plane. *Systems & Control Letters* 2007; **56**(9-10):573 – 578.
2. Dimarogonas DV, Johansson KH. On the stability of distance-based formation control. *Proceedings of the 47th IEEE Conference on Decision and Control*, 2008; 1200–1205.
3. Yu C, Anderson BDO, Dasgupta S, Fidan B. Control of minimally persistent formations in the plane. *SIAM Journal on Control and Optimization* 2009; **48**(1):206–233.
4. Krick L, Broucke ME, Francis BA. Stabilisation of infinitesimally rigid formations of multi-robot networks. *International Journal of Control* 2009; **82**:423–439.
5. Ren W, Sorensen N. Distributed coordination architecture for multi-robot formation control. *Robotics and Autonomous Systems* 2008; **56**(4):324–333.
6. Moshtagh N, Michael N, Jadbabaie A, Daniilidis K. Vision-based, distributed control laws for motion coordination of nonholonomic robots. *IEEE Transactions on Robotics* 2009; **25**(4):851–860.
7. Basiri M, Bishop AN, Jensfelt P. Distributed control of triangular formations with angle-only constraints. *Systems & Control Letters* 2010; **59**(2):147 – 154.
8. Fax J, Murray R. Information flow and cooperative control of vehicle formations. *IEEE Transactions on Automatic Control* 2004; **49**(9):1465–1476.
9. Olfati-Saber R, Murray R. Consensus problems in networks of agents with switching topology and time-delays. *IEEE Transactions on Automatic Control* 2004; **49**(9):1520–1533.
10. Anderson BDO, Yu C, Fidan B, Hendrickx JM. Rigid graph control architectures for autonomous formations. *IEEE Control Systems Magazine* 2008; **28**(6):48–63.
11. Olfati-Saber R, Murray R. Graph rigidity and distributed formation stabilization of multi-vehicle systems. *Proceedings of the 41st IEEE Conference on Decision and Control*, vol. 3, 2002; 2965–2971.
12. Wachter LM, Ray LE. Stability of potential function formation control with communication and processing delay. *Proceedings of the 48th conference on American Control Conference*, 2009; 2997–3004.
13. Secchi C, Fantuzzi C. Formation control over delayed communication networks. *IEEE International Conference on Robotics and Automation*, 2008; 563–568.
14. Weimerskirch H, Martin J, Clerquin Y, Alexandre P, Jiraskova S. Energy saving in flight formation. *Nature* 2001; **413**(6857):697– 698.
15. Bishop A, Anderson BDO, Fidan B, Pathirana PN, Mao G. Bearing-only localization using geometrically constrained optimization. *IEEE Transactions on Aerospace and Electronic Systems* 2009; **45**(1):308–320.
16. Bishop AN, Fidan B, Anderson BDO, Doğançay K, Pathirana PN. Optimality analysis of sensor-target localization geometries. *Automatica* 2010; **46**(3):479–492.
17. Doğançay K, Hmam H. Optimal angular sensor separation for AOA localization. *Signal Processing* 2008; **88**(5):1248–1260.
18. Zhang F, Leonard N. Generating contour plots using multiple sensor platforms. *Proceedings of 2005 IEEE Swarm Intelligence Symposium*, 2005; 309 – 316.
19. Spletzer J, Fierro R. Optimal positioning strategies for shape changes in robot teams. *Proceeding of IEEE International Conference on Robotics and Automation*, 2005; 742–747.
20. Bhatt RM, Tang CP, Krovi VN. Formation optimization for a fleet of wheeled mobile robots – a geometric approach. *Robotics and Autonomous Systems* 2009; **57**(1):102 – 120.
21. Pais D, Cao M, Leonard N. Formation shape and orientation control using projected collinear tensegrity structures. *Proceedings of the 2009 American Control Conference*, 2009; 610 – 615.
22. Kim DY, Woo B, Park SY, Choi KH. Hybrid optimization for multiple-impulse reconfiguration trajectories of satellite formation flying. *Advances in Space Research* 2009; **44**(11):1257 – 1269.
23. Tillerson M, Inalhan G, How JP. Co-ordination and control of distributed spacecraft systems using convex optimization techniques. *International Journal of Robust and Nonlinear Control* 2002; **12**(2-3):207 – 242.
24. Diestel R. *Graph Theory, Graduate Texts in Mathematics*, vol. 173. Fourth edn., Springer-Verlag, Heidelberg, 2010.
25. Dörfler F, Francis B. Formation control of autonomous robots based on cooperative behavior. *Proceedings of the European Control Conference 2009*, Budapest, Hungary, 2009; 2432–2437.
26. Huttenlocher DP, Klanderma GA, Rucklidge WA. Comparing Images Using the Hausdorff Distance. *IEEE Transaction on Pattern Analysis and Machine Intelligence* 1993; **15**(9):850–863.
27. Huang H, Yu C, Wu Q. Distributed LQR design for multi-agent formations. *Proceedings of the 49th IEEE Conference on Decision and Control*, 2010; 4535 – 4540.
28. Anderson BDO, Fidan B, Yu C, Walle DVD. Autonomous UAV formation: Theory and application. *Recent Advances in Learning and Control, Lecture Notes in Control and Information Sciences*, vol. 371, Blondel VD, Boyd S, Kimura H (eds.), Springer, 2008; 15–33.
29. Belta C, Kumar V. Optimal motion generation for groups of robots: A geometric approach. *Journal of Mechanical Design* 2004; **126**(1):63–70.
30. Anderson BDO, Belhumeur P, Eren T, Goldenberg D, Morse A, Whiteley W, Yang Y. Graphical properties of easily localizable sensor networks. *Wireless Networks* 2009; **15**(2):177–191.
31. Kalantar S, Zimmer U. Scale-adaptive polygonal formations of submersible vehicles and tracking isocontours. *IEEE/RSJ International Conference on Intelligent Robots and Systems*, 2008; 3146–3151.
32. Doğançay K. Bearings-only target localization using total least squares. *Signal Process.* 2005; **85**(9):1695–1710.
33. Martinez S, Bullo F. Optimal sensor placement and motion coordination for target tracking. *Automatica* 2006; **42**(4):661 – 668.
34. Dogancay K. Online optimization of receiver trajectories for scan-based emitter localization. *IEEE Transactions on Aerospace Electronic Systems* 2007; **43**(3):1117–1125.